Observational Study

Medicine

OPEN

Predictive value of MR imaging IVIM and T2 mapping in malignant transformation of endometriosis

Simeng Liu, MM[a], Miao Peng, MM[a], Runze Yu, MM[a], Cuicui Jin, MM[a], Shanshan Zhou, MB[a], Yuhui Deng, MD[a], Deli Zhao, MD[a,*]

Abstract

This study aims to explore the value of MRI intravoxel incoherent motion (IVIM) combined with T2 mapping in predicting the malignancy of endometriosis (EM) and construct a noninvasive preoperative risk assessment model. A retrospective analysis was conducted on 156 patients with pathologically confirmed EM or endometriosis - associated ovarian cancer, who were divided into the benign group (102 cases) and the malignant transformation group (54 cases). Two observers independently measured the IVIM parameters (D, D*, f) and T2 values to construct single-parameter and multi-parameter joint models. The receiver operator characteristic curve was used to evaluate the diagnostic efficacy, and logistic regression was used to analyze the independent predictors. The values of D, f, and T2 in the malignant transformation group were significantly lower than those in the benign group (all $P < .05$), while there was no statistically significant difference in D* value. The area under curve (AUC) of D, f, T2, and the combined model D + f + T2 were 0.737, 0.701, 0.773, and 0.874, respectively. The optimal cutoff values of D, f, and T2 were 1.10×10^{-3} mm^2/s, 37.30 %, and 119.65 ms, respectively. Values lower than these may indicate a risk of malignant transformation of EM. Logistic regression confirmed that D, D*, and T2 were independent predictors of EM malignancy. IVIM combined with T2 mapping can non-invasively and quantitatively assess the risk of malignant transformation of EM. The combined model of parameters of two sequences has good potential for clinical promotion.

Abbreviations: AUC = area under curve, CI = confidence interval, D = ture-diffusion coefficient, D* = pseudo-diffusion coefficient, DWI = diffusion-weighted imaging, EAOC = endometriosis-associated ovarian cancer, EC = endometrial carcinoma, EM = endometriosis, f = microcirculation perfusion fraction, HE4 = human epididymis protein 4, IVIM = intravoxel incoherent motion, LGSC = low-grade serous ovarian cancer, mpMRI = multiparametric magnetic resonance imaging, OCCC = ovarian clear cell carcinoma, OEC = ovarian endometrioid carcinoma, OR = odds ratio, ROI = region of interest, T1WI = T1-weighted imaging, T2WI = T2-weighted imaging, VIF = variance inflation factor.

Keywords: endometriosis, intravoxel incoherent motion, magnetic resonance imaging, malignant transformation, T2 mapping

1. Introduction

Endometriosis (EM) is a common gynecological disease that affects approximately 10% to 15% of women of childbearing age.[1] Although EM is a typical benign disease, it has the risk of malignant transformation. Current literature reports that the probability is about 1%,[2] but due to various limitations, its actual malignant transformation rate should be much higher than this. EM can undergo malignant transformation into endometriosis-associated ovarian cancer (EAOC), which accounts for approximately 10% to 15% of all ovarian cancers.[3] The main histopathological subtypes of EAOC include endometrioid ovarian carcinoma (OEC, accounting for approximately 50–60%), clear cell ovarian carcinoma (OCCC, about 20–30%), and other rare types such as low-grade serous ovarian cancer (LGSC, about 10–20%).[4] Due to the large number of EM patients, the number of EAOC cannot be ignored. At present, the diagnosis of malignant transformation of EM in clinical practice mainly relies on postoperative pathological confirmation. At this stage, the tumor often shows obvious malignant morphological manifestations and has developed to a higher grade. However, in the early stage of malignant transformation, many EM lesions

YD and DZ contributed equally to this work.

This work was supported by the Key Research and Development Program Project of Heilongjiang Province (grant no. 2023ZX06C13) and the National Natural Science Foundation of China (grant no. 82502472).

The authors have no conflicts of interest to disclose.

The datasets generated during and/or analyzed during the current study are available from the corresponding author on reasonable request.

This study was approved by the Ethics Committee of the Sixth Affiliated Hospital of Harbin Medical University (no. LC2024-147). According to the Helsinki Declaration, patients are exempted from the informed consent form.

[a] *Department of Radiology, The Sixth Affiliated Hospital of Harbin Medical University, Harbin, China.*

* *Correspondence: Deli Zhao, Department of Radiology, The Sixth Affiliated Hospital of Harbin Medical University, No. 998, Aiying Street, Songbei District, Harbin, Heilongjiang Province 150000, China (e-mail: delizhao_123@163.com).*

How to cite this article: Liu S, Peng M, Yu R, Jin C, Zhou S, Deng Y, Zhao D. Predictive value of MR imaging IVIM and T2 mapping in malignant transformation of endometriosis. Medicine 2025;104:51(e46665).

Received: 17 August 2025 / Received in final form: 23 October 2025 / Accepted: 27 October 2025

http://dx.doi.org/10.1097/MD.0000000000046665

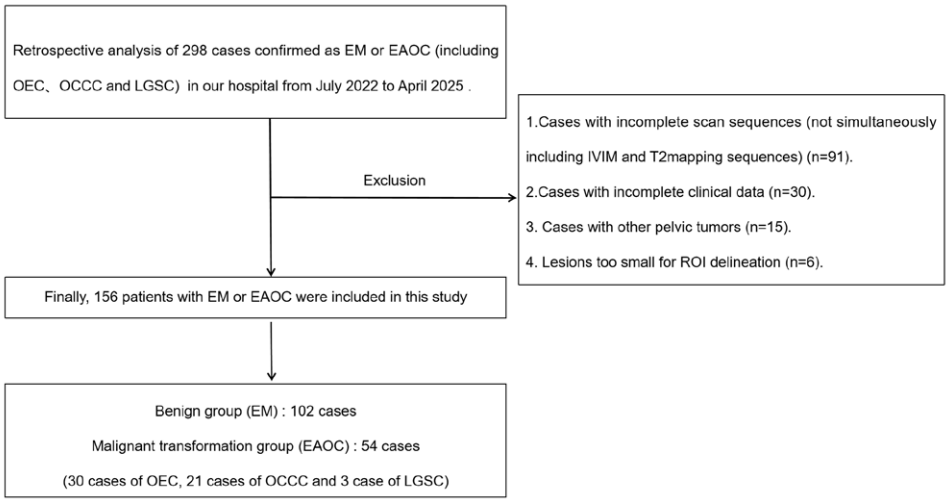

Figure 1. Enrollment flow chart. EAOC = endometriosis-associated ovarian cancer, EM = endometriosis, IVIM = intravoxel incoherent motion, LGSC = low-grade serous ovarian cancer, OCCC = ovarian clear cell carcinoma, OEC = ovarian endometrioid carcinoma, ROI = region of interest.

have not undergone significant morphological changes, which often leads to the neglect of these early malignant transformation cases in clinical practice and the lack of effective strategies and methods to monitor the disease status. Therefore, how to achieve the early diagnosis of malignant transformation of EM has become an urgent problem to be solved in clinical practice.

Multi-parameter magnetic resonance imaging (mpMRI), which combines multiple anatomical and functional sequences in a single examination, offers a potential solution. It can non-invasively, multimodal and highly sensitively assess the morphology, blood flow, metabolism and microenvironment of lesions.[5] It has been widely used in lesions of various systems. Intravoxel incoherent motion (IVIM) is an advanced functional subtype of diffusion-weighted imaging (DWI). It uses a single-shot echo planar imaging sequence with multiple b-values to simultaneously extract the true-diffusion coefficient (D), pseudo-diffusion coefficient (D*) and microcirculation perfusion fraction (f) of tissue through a double-exponential model, obtaining quantified perfusion information without the need for contrast agents.[6] Previous studies have confirmed that this sequence can not only distinguish benign and malignant ovarian tumors, differentiate type I and type II epithelial ovarian cancer, but also predict the Ki-67 index of ovarian cancer before surgery.[7–9] Corresponding to the "function-perfusion" perspective of IVIM, T2 mapping provides pure quantitative relaxation information. It fits the T2 value of each voxel through multi-echo T2WI, directly reflecting the free water content and microstructure changes of the tissue.[10] In uterine lesions, significant differences in T2 values have been used for differentiating benign and malignant conditions and monitoring therapeutic effects.[11] Therefore, IVIM and T2 mapping will respectively evaluate the pathological state of EM lesions from the aspects of "perfusion" and "quantification."

This study aims to investigate the predictive value of IVIM and T2 Mapping sequences in the malignant transformation of endometriosis (EM). We plan to develop a noninvasive, convenient and repeatable multi-parameter assessment tool to identify the malignant transformation of EM at an early stage, thereby improving the long-term prognosis of malignant tumors.

2. Materials and methods

2.1. Study population

This study was approved by the Institutional Review Board of the Sixth Affiliated Hospital of Harbin Medical University (IRB#LC-2024-147). Patients were exempted from signing the informed consent form. A retrospective collection was made of 298 patients who were pathologically confirmed to have EM or EAOC (including OEC, OCCC, and LGSC) underwent 3.0T MRI examination in our hospital from July 2022 to April 2025. Exclusion criteria: Cases with incomplete scan sequences (not simultaneously including IVIM and T2mapping sequences) (n = 91). Cases with incomplete clinical data (n = 30). Cases with other pelvic tumors (n = 15). Lesions too small for region of interest (ROI) delineation (n = 6). Ultimately, 156 patients were included, among whom 102 were EM patients (benign group) and 54 patients with EAOC (malignant transformation group), including 30 cases of OEC, 21 cases of OCCC, and 3 case of LGSC. The enrollment process is shown in Figure 1.

2.2. Clinical data

The clinical data collected included age, maximum tumor diameter, symptoms (dysmenorrhea or chronic pelvic pain), menopausel state (before menopause or after menopause), carbohydrate antigen 125 (CA125, U/mL), human epididymis protein 4 (HE4, pmol/mL), and risk of ovarian malignancy algorithm index.

2.3. MRI imaging

A 3.0T MRI scanner (Siemens 3.0T MRI, Skyra, Germany) with a 18-channel abdominal coil was used. Patients emptied their bladder and fasted for 4 to 6 hours before the scan. The scanning sequences included conventional T1WI and T2WI, as well as IVIM and T2 mapping. IVIM used single-shot echo planar imaging sequence with 12 b-values (0, 30, 50, 100, 150, 200, 400, 600, 800, 1200, 1500, 2000 s/mm²). T2 mapping used gradient echo spin echo technology to acquire 5 echo signals ($TE_{1\text{-}5}$ = 20, 40, 60, 80, 100 ms). Scan parameters are shown in Table 1.

2.4. Image analysis

The IVIM sequences were extracted through medical data processing software (MITK), and the T2mapping sequences were analyzed through the post-processing workstation (Syngo. via). Two radiologists, with 15 years and 8 years of experience in pelvic radiological diagnosis respectively, determined the lesion location by referencing axial T2WI or DWI. In cases of disagreement, a consensus was reached through consultation,

Table 1

MRI scan sequences and parameters.

Parameters	Scan time (min)	TR (ms)	TE (ms)	Matrix	FOV (mm^2)	Thickness (mm)	Gap (mm)
T1WI (DIXON)	14 s	3.96	1.26	130 × 130	400 × 400	2.3	0.5
T2WI	1 min 46 s	4080	85	30 × 30	220 × 220	4.0	1.2
IVIM	6 min 55 s	8500	77	110 × 110	250 × 250	4.0	1.2
T2 mapping	2 min 54 s	1500	20–100	50 × 50	250 × 250	4.0	0.2

IVIM with b value of 0, 30, 50, 100, 150, 200, 400, 600, 800, 1200, 1500, 2000 s/mm^2. The number of excitations for each b value is once.
DIXON = a type of T1WI sequence, FOV = field of view, T2WI = T2-weighted imaging, TE = echo time, TR = time of repetition.

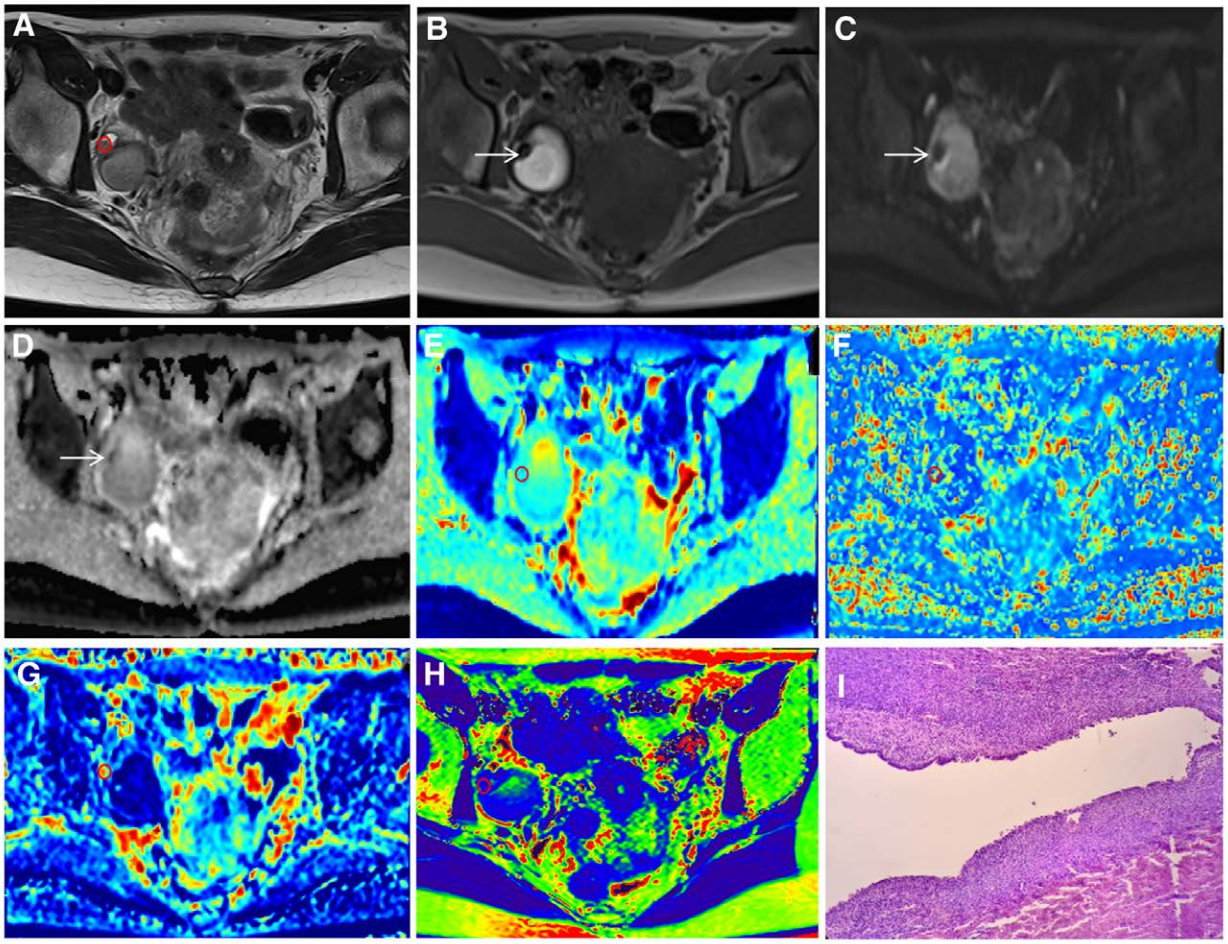

Figure 2. A 28-year-old with EM of right ovary, pathology confirmed the presence of blood clots adhered to the cyst wall. (A) T2WI, (B) T1WI, (C) IVIM's standard high-b DWI, (D) ADC (b = 800s/mm^2), (E) D-parameter diagram, (F) D*-parameter diagram, (G) f-parameter diagram, (H) T2 mapping map. A–H showed the ROI delineation (red circle) of the solid part in the cystic lesion of the right adnexal area; D, D*, f, and T2 values were 1.19 × $10^{-3}$$mm^2$/s, 31.93 × $10^{-3}$$mm^2$/s, 45.7%, and 138.26 ms, respectively. (I) Pathologic figure of HE staining (HE × 200). ADC = apparent diffusion coefficient, D = ture-diffusion coefficient, D* = pseudo-diffusion coefficient, DWI = diffusion-weighted imaging, f = microcirculation perfusion fraction, IVIM = intravoxel incoherent motion, ROI = region of interest, T1WI = T1-weighted imaging, T2WI = T2-weighted imaging.

with the final decision made by the senior radiologist. Based on the T2WI sequence to determine ROI, which was then replicated to the corresponding levels of the D, D*, f, and T2 mapping parameter maps. The selection of the ROI is strictly limited to the solid part of the tumor or the thickest part of the cyst wall (thickness > 3 mm), while avoiding the cystic part and the bleeding area. For typical hemorrhagic cysts without obvious wall thickening in the benign group, researchers delineated ROI on the cyst walls to avoid the obvious artifacts caused by the T2* effect. The size of ROI is defined as a circular area, which is between 50% and 90% of the target area, ensuring that it contains most of the solid part of the lesion while avoiding the liquid part around it, to meet the needs of lesions of different sizes (Figs. 2 and 3). All ROIs were manually defined by 2 experienced radiologists, and the consistency among operators was evaluated using the intra-group correlation coefficient (ICC).

2.5. Statistical analysis

Statistical analysis was performed using SPSS 27.0 and GraphPad Prism 10 software. The ICC was used to evaluate the consistency of the measurement values between the two observers. The Shapiro–Wilk test was used to evaluate the normality of clinical data and MRI quantitative parameters.

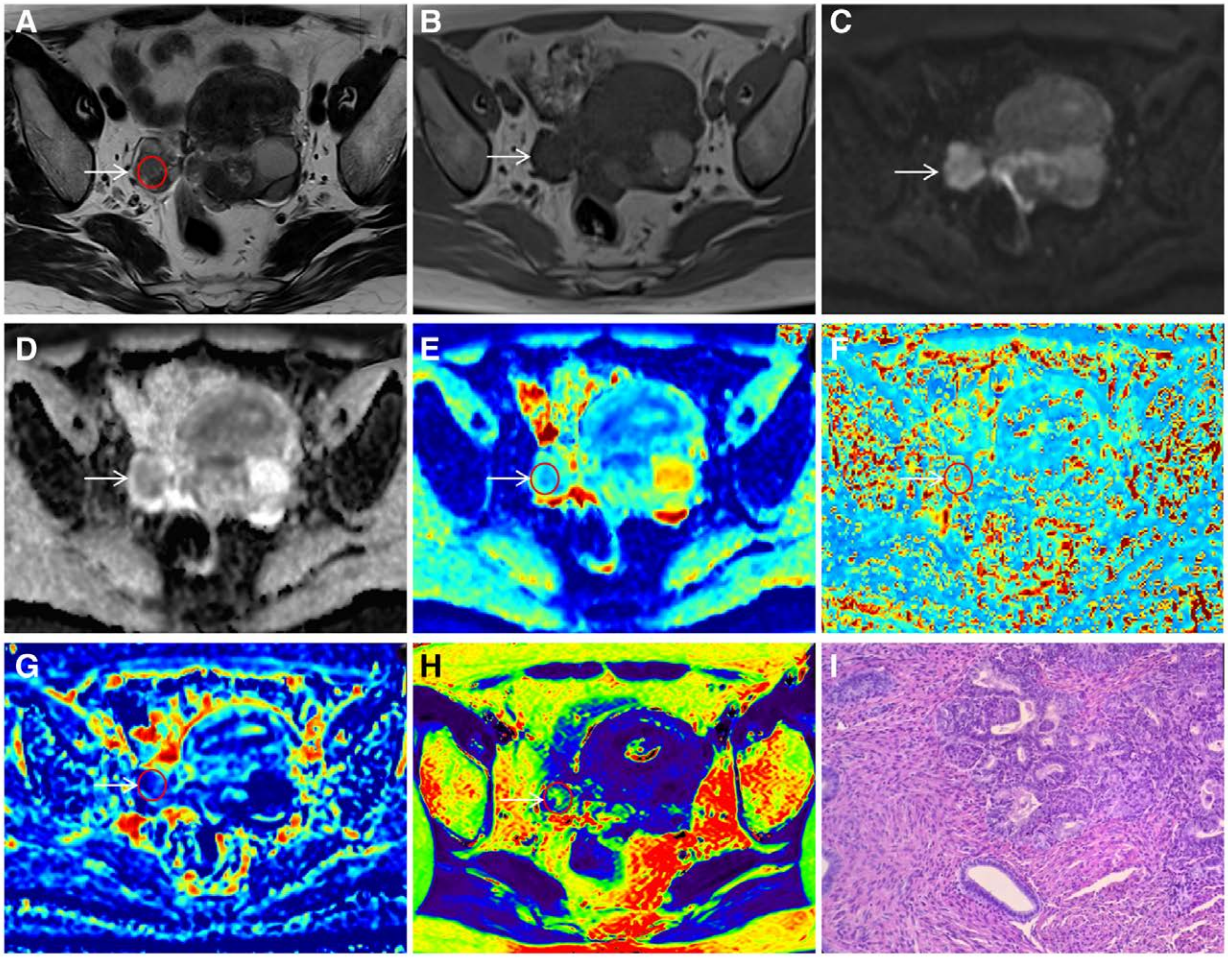

Figure 3. A 47-year-old with EOC of bilateral ovaries. (A) T2WI, (B) T1WI, (C) IVIM's standard high-b DWI, (D) ADC (b = 800 s/mm^2), (E) D-parameter diagram, (F) D*-parameter diagram, (G) f-parameter diagram, (H) T2 mapping map. A-H showed the ROI delineation (red circle) of the solid part in the lesion of the right adnexal area; D, D*, f, and T2 values were 0.53 × 10^{-3}mm^2/s, 35.42 × 10^{-3}mm^2/s, 29.8%, and 109.23 ms, respectively. (I) Pathologic figure of HE staining (HE × 200). ADC = apparent diffusion coefficient, D = ture-diffusion coefficient, D* = pseudo-diffusion coefficient, DWI = diffusion-weighted imaging, f = micro-circulation perfusion fraction, IVIM = intravoxel incoherent motion, ROI = region of interest, T1WI = T1-weighted imaging, T2WI = T2-weighted imaging.

Data conforming to a normal distribution were expressed as x ± s, and data not conforming to a normal distribution were expressed as 50% (25%, 75%). Count data were analyzed using the independent sample *t* test or the Mann–Whitney *U* test, and measurement data were analyzed using the chi-square test or Fisher's exact probability method to compare the parameter differences between the 2 groups. The diagnostic efficacy of each parameter model was analyzed through the receiver operating characteristic curve, and the DeLong test was used to compare the differences in the area under the curve (AUC) among different models. The correlation between the 2 independent parameters was tested by the Spearman correlation coefficient. For the clinical data with differences and all quantitative parameters, the independent predictors of malignant transformation of EM were evaluated by the method of binary Logistic regression first and then multiple Logistic regression analysis. The variance inflation factor was used to conduct collinearity checks on each variable.

3. Results

3.1. Comparison of clinical data

The clinical characteristics of 102 benign cases and 54 malignant transformation cases were compared. There were no statistically significant differences in age, maximum tumor diameter, symptoms of dysmenorrhea or chronic pelvic pain, menopausal status, CA125 level and risk of ovarian malignancy algorithm index (all $P > .05$). However the serum HE4 level in the malignant transformation group was significantly higher than that in the benign group (60.85 ± 13.29 vs 49.20 ± 4.38 pmol/mL, $P = .002$), suggesting that the increase of HE4 might be a potential marker of malignant transformation. (as shown in Table 2).

3.2. Parameter measurement consistency

The repeatability of the measurements of IVIM-DWI and T2 parameters by the two observers was good in both the benign and malignant transformation groups. In the benign group (n = 102), the ICCs of D, D*, f, and T2 values were 0.840, 0.893, 0.854, and 0.827, respectively; In the malignant transformation group (n = 54), they were 0.910, 0.845, 0.821, and 0.784, all of which were ≥ 0.75. The differences in the average values of each parameter between the 2 groups were relatively small, suggesting that the measurement results were stable and reliable (Table 3).

3.3. Parameter difference comparison

The results showed that there were statistically significant differences in D value, f value, and T2 value between the benign

group and the malignant transformation group, while there was no statistically significant difference in D* value. Specifically, the D value of the benign group ($1.102 \pm 0.81 \times 10^{-3}$ mm²/s) was significantly higher than that of the malignant transformation group ($0.69 \pm 0.29 \times 10^{-3}$ mm²/s, $t = 4.182$, $P < .001$); The f value was also significantly higher than that of the malignant transformation group (39.99% ± 12.01% vs 31.75% ± 7.39%, $t = 3.0156$, $P = .004$); The T2 value was also significantly higher than that of the malignant transformation group (122.85 ± 7.03 vs 113.91 ± 9.13 ms, $t = 3.928$, $P < .001$). On the contrary, there was no statistically significant difference in D* values between the 2 groups ($P = .087$) (Table 4; Fig. 4).

3.4. Diagnostic efficacy evaluation

The AUC values of different models D, f, T2, D + f, D + T2, f + T2, and D + f + T2 identified between the 2 groups were 0.737, 0.701, 0.773, 0.791, 0.856, 0.843, and 0.874, respectively. Under this scanning condition, the cutoff values of the D, f, and T2 parameters for the malignant transformation of EM were 1.10×10^{-3} mm²/s, 37.30%, and 119.65 ms, respectively. If lower than these values, suggesting the possibility of malignant transformation of EM (as shown in Table 5; Fig. 5). The De-Long test was used to conduct pairwise comparisons one by one between the single-parameter model (D, f, T2) and the combined model D + f + T2, as well as between the two-parameter model (D + T2) with the highest diagnostic efficacy and the combined model (D + f + T2). The result revealed that the combined model (D + f + T2) demonstrated a statistically significant improvement in AUC compared to the f-only model ($P = .0442$) and a trend towards improvement compared to the D-only model ($P = .0974$). (as shown in Table 6).

3.5. Correlation analysis

D and f values were moderately positively correlated ($r = 0.4576$, $P = .0006$), D and T2 values weakly positively correlated ($r = 0.3356$, $P = .0150$), with no significant correlation between f and T2 values ($P > .05$), as shown in Figure 6.

3.6. Regression analysis

The results of univariate and multivariate analyses between the benign group and the malignant transformation group showed that at the univariate level, the 4 indicators of HE4, D, D*, and T2 were all significantly correlated with malignant transformation, while the f value did not reach statistical significance ($P = .086$). After entering the multi-factor model, only D, D*, and T2 values still independently indicated the risk of malignant transformation: a decrease in D value (odds ratio [OR] = 0.783), an increase in D* value (OR = 1.426) and a decrease in T2 value (OR = 0.839) were all significantly associated with malignant transformation, while HE4 no longer had independent predictive value ($P = .397$) (as shown in Table 7). Interestingly, while D* was not significantly different between groups in univariate analysis, it emerged as an independent predictor in the multivariate model, suggesting its predictive value may be contingent

Table 2

Analysis of clinical characteristics.

Clinical characteristics	Benign group (n = 102)	Malignant transformation group (n = 54)	*P*
Age (year)	44.6 ± 9.5	48.7 ± 8.0	.126*
Maximum diameter of the tumor (mm)	25.2 ± 9.0	25.4 ± 8.8	.939*
Symptoms of dysmenorrhea or chronic pelvic pain, n (%)			.492*
Yes	59 (57.8)	35 (64.8)	
No	43 (42.2)	19 (35.2)	
Menopause status, n (%)			.112†
Before	71 (69.6)	30 (55.6)	
After	31 (30.4)	24 (44.4)	
CA125 (U/mL)	17.0 (9.2, 23.2)	17.3 (9.5, 25.4)	.758‡
HE4 (pmol/mL)	49.20 ± 4.38	60.85 ± 13.29	.002*
ROMA (%)	10.9 ± 5.4	11.1 ± 6.1	.883*

CA125 = carbohydrate antigen 125 (normal reference range: 0–35 U/mL); HE4 = human epididymis protein 4 (normal reference range: before menopause 0–92.1 pmol/mL; after menopause 0–121 pmol/mL); ROMA = Risk of Ovarian Malignancy Algorithm (normal reference range: before menopause <11.4%; after menopause <29.9%).

*Data analyzed using the independent samples *t* test.

†Data analyzed using the chi-square test.

‡Data analyzed using the Mann–Whitney *U* test.

Table 3

Agreement analysis of the values of each parameter measured by the 2 observers.

	Observer1	Observer2	ICC
Benign group (n = 102)			
D ($\times 10^{-3}$mm²/s)	1.26 ± 0.79	1.36 ± 0.81	0.840
D* ($\times 10^{-3}$mm²/s)	31.76 ± 8.49	32.15 ± 8.79	0.893
F (%)	39.0 ± 12.1	40.9 ± 12.0	0.854
T2 (ms)	122.19 ± 7.39	123.62 ± 7.81	0.827
Malignant transformation group (n = 54)			
D ($\times 10^{-3}$mm²/s)	0.63 ± 0.22	0.73 ± 0.32	0.910
D* ($\times 10^{-3}$mm²/s)	35.89 ± 5.83	35.06 ± 5.01	0.845
f (%)	31.9 ± 7.5	31.2 ± 7.0	0.821
T2 (ms)	111.92 ± 8.77	114.74 ± 7.57	0.784

D = ture-diffusion coefficient, D* = pseudo-diffusion coefficient, f = microcirculation perfusion fraction, ICC = Intraclass correlation coefficient (ICC < 0.40, 0.40 ≤ ICC < 0.75 and ICC ≥ 0.75 were regarded as poor, medium and good consistency, respectively).

Table 4

Analysis of the differences in the values of each parameter between the 2 groups of cases.

	Benign group (n = 102)	Malignant transformation group (n = 54)	*t*	*P*
D ($\times 10^{-3}mm^2/s$)	1.34 ± 0.81	0.69 ± 0.29	4.182	<.001
D* ($\times 10^{-3}mm^2/s$)	32.01 ± 8.74	35.35 ± 5.06	−1.745	.087
f (%)	39.9 ± 12.0	31.7 ± 7.3	3.052	.004
T2 (ms)	122.85 ± 7.03	113.91 ± 9.13	3.928	<.001

D = ture-diffusion coefficient, D* = pseudo-diffusion coefficient, f = microcirculation perfusion fraction.

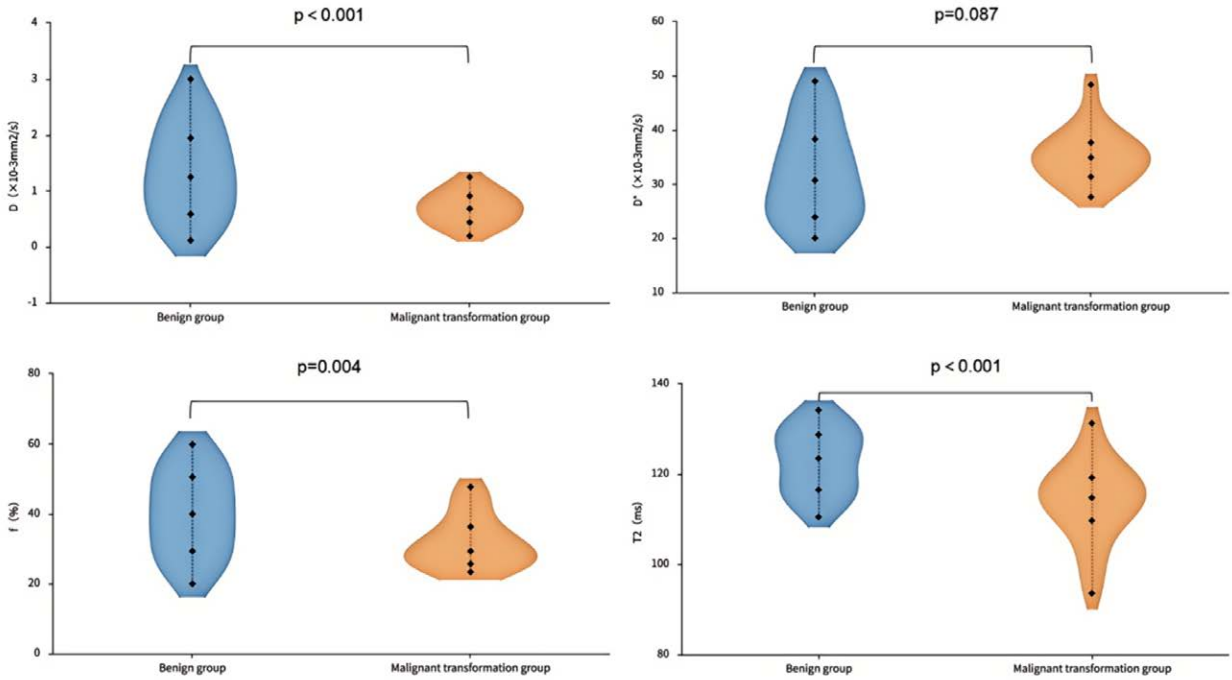

Figure 4. Comparison of parameter values between cases in the benign group and malignant transformation group.

Table 5

Assessment of the efficacy of each parameter alone or in combination to identify the 2 groups of cases.

Parameters	AUC (95% CI)	Sensitivity (%)	Specificity (%)	cutoff
D	0.737 (0.604–0.870)	58.8	94.4	$1.10 \times 10^{-3}mm^2/s$
f	0.701 (0.560–0.842)	55.9	83.3	37.30%
T2	0.773 (0.639–0.907)	61.8	83.3	119.65ms
D + f	0.791 (0.670–0.912)	59.3	61.8	–
D + T2	0.856 (0.756–0.957)	88.9	70.6	–
f + T2	0.843 (0.736–0.951)	88.4	70.9	–
D + f + T2	0.874 (0.781–0.967)	83.3	82.4	–

AUC = area under curve, CI = confidence interval.

on its relationship with other parameters like D and T2. This finding requires further validation. The results of covariance test showed that the variance inflation factor of HE4, D, D*, f, and T2 values were 2.045, 1.721, 1.643, 1.260, and 1.444, respectively, which were < 5, indicating that the factors were independent of each other.

4. Discussion

EM malignancy is caused by multiple factors, including hormones, inflammation, oxidative stress, gene mutations, and epigenetic changes.[12] CYP1B1 overexpression in ectopic endometrium converts androstenedione to estrogen, causing DNA damage and cell proliferation, while menstrual blood reflux induces iron imbalance and oxidative stress, leading to DNA damage, cellular dysfunction, and angiogenesis, ultimately promoting malignancy.[13,14] The microenvironment of tumors can affect the phenotypic transformation of tumors and increase the heterogeneity of malignant tumors, playing an important role in the malignant transformation of EM. mpMRI technology can comprehensively and dynamically evaluate the characteristics of the tumor microenvironment and provide a variety of information related to the biological behavior and metabolic state of tumors. The research of Li et al[15] has confirmed the value of multimodal MRI imaging in predicting the expression of Her-2 gene in endometrial cancer, and the diagnostic efficacy of its combined model is 0.860. This study used D, D*, f values from

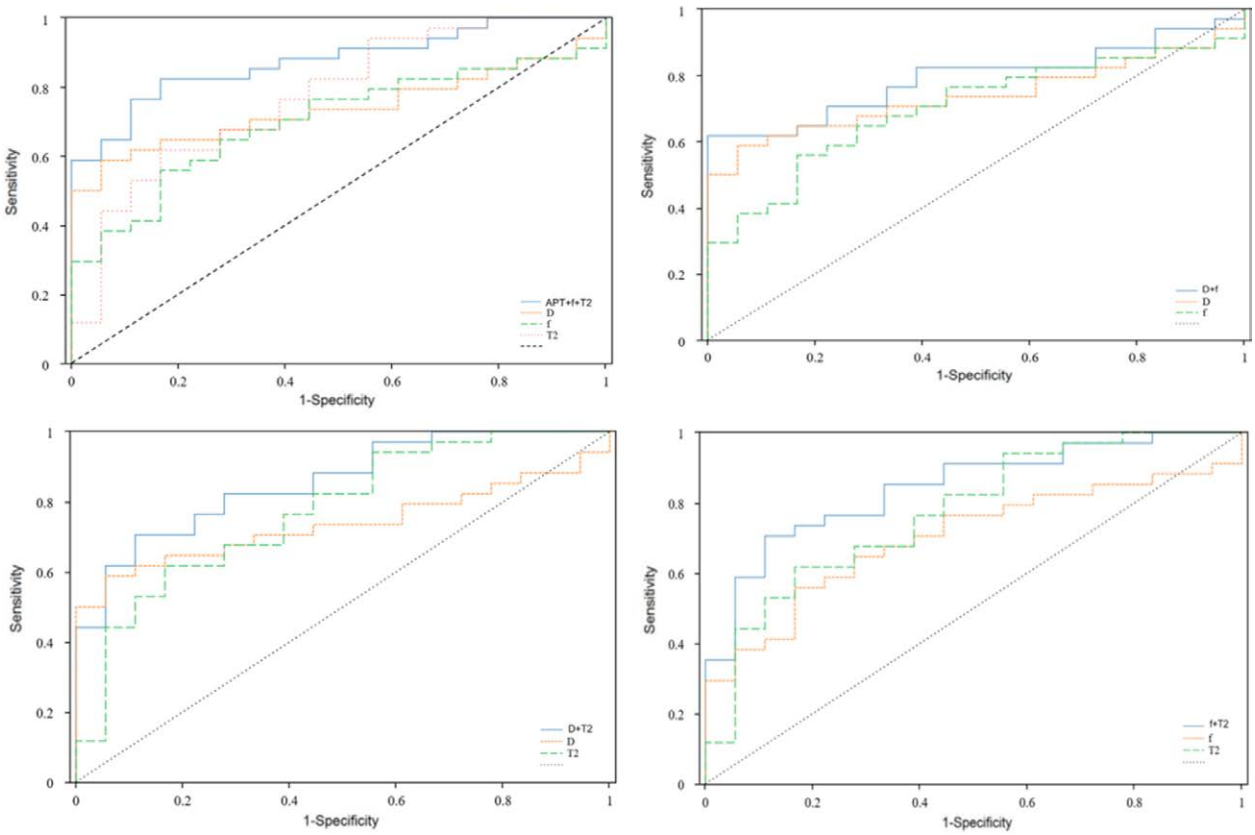

Figure 5. ROC curve of D, f, T2, and combined parameters model to identify the 2 groups of cases. D = ture-diffusion coefficient, f = microcirculation perfusion fraction, ROC = receiver operator characteristic.

Table 6

Results of ROC comparisons for different parameters.

Parameter comparison	D + f + T2 vs D	D + f + T2 vs f	D + f + T2 vs T2	D + f + T2 vs D + T2
Z-statistic	1.4045	2.0120	0.9673	0.2595
P value	.0974	.0442	.2264	.7952

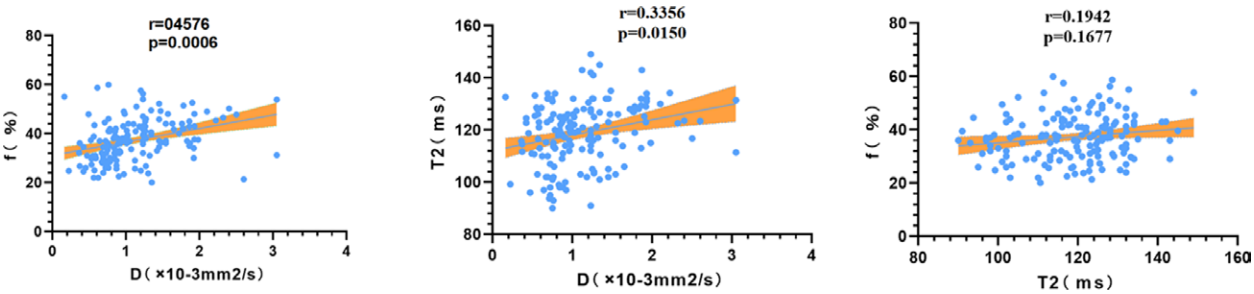

Figure 6. Correlation analysis graph for each individual difference parameter.

IVIM and T2 values from T2 mapping to predict endometrial malignancy transformation, achieving a predictive efficiency of 0.874 with high accuracy.

Histopathological examination (histological assessment under a microscope) has always been the gold standard for judging the malignant transformation of EM into EAOC and its specific pathological subtypes. However, pathological examination requires obtaining tissue samples through surgery or puncture, a process that is invasive and may cause additional pain and risks to patients. Moreover, in some cases, the obtained tissue samples may not be sufficient for accurate pathological analysis.[16,17] In view of this, it is particularly important to explore a method that can predict the malignant transformation of EM in real time and non-invasively. At present, there are studies attempting to utilize imaging techniques to solve this problem. Zheng et al[16] attempted to use contrast-enhanced ultrasound imaging to evaluate the blood perfusion of EM lesions in order to predict their malignant transformation potential. However, this method has a high technical dependence on the operator and limited specificity. Furthermore, Phulia et al[17] proposed the use

Table 7

Univariate and multifactorial analysis of benign group and malignant transformation group.

	Univariate analyses		Multivariate analyses	
Parameters	**OR (95% CI)**	***P* value**	**OR (95% CI)**	***P* value**
HE4 (pmol/mL)	1.156 (1.057–1.265)	.002	1.057 (0.930–1.202)	.397
D ($\times10^{-3}mm^2/s$)	0.776 (0.701–0.822)	.007	0.783 (0.703–0.849)	.023
D* ($\times10^{-3}mm^2/s$)	1.617 (1.177–2.220)	.003	1.426 (1.020–1.994)	.038
f (%)	0.885 (0.770–1.017)	.086	/	/
T2 (ms)	0.806 (0.707–0.919)	.001	0.839 (0.712–0.988)	.035

CI = confidence interval, HE4 = human epididymis protein 4, OR = odds ratio.

of positron emission tomography (PET) combined with CT to evaluate the metabolic activity of EM lesions. However, PET-CT examination is expensive, has a large radiation dose, and still has deficiencies in specificity, making it difficult to be widely used in clinical practice.

Development of mpMRI technology has brought new hope to this field. As a noninvasive MR Imaging technique at the molecular level, IVIM imaging can reflect the microstructure of tissues and blood perfusion information by measuring diffusion and perfusion parameters.[18] IVIM technology is based on a double-exponential model and separates the molecular diffusion and microcirculation perfusion information within tissues through DWI. Its core parameters include D, D*, and f.[19] The IVIM signal can not only reflect diffusion characteristics of tissue, but also demonstrate the microvessel density and blood perfusion conditions. Tao et al[20] directly compared MRI images and pathological sections through animal model experiments and confirmed that various parameters of IVIM can effectively evaluate microangiogenesis of tumors and truly reflect vascular endothelial structure state and perfusion conditions. A key advantage of IVIM is its ability to provide quantitative information on tissue perfusion without the need for contrast-agent administration. It is particularly suitable for patients who cannot tolerate gadolinium contrast agents and has the advantages of low cost and wide applicability. Arian et al[21] studied that in differentiating benign and malignant breast lesions, IVIM and dynamic contracontra-enhanced (DCE) had similar sensitivity (86.2% vs 93.8%), but in terms of specificity (70.3% vs 68.1%), IVIM was even slightly superior to DCE imaging. In previous multiple studies, IVIM parameters can significantly distinguish head and neck tumors of different pathological types.[22] In the diagnosis of breast lesions compared with traditional DWI, IVIM can quantify cell density and vascularization degree respectively.[23] In the field of liver diseases, IVIM technology has been used to evaluate nonalcoholic fatty liver disease, liver fibrosis and liver tumors.[24]

The results of this study show that in the malignant transformation group of EM, D value and f value of IVIM sequence were significantly lower than those in the benign group, while there was no statistically significant difference in the D* value. The possible reason for this is as follows: Firstly, during the malignant transformation of benign EM lesions, the D value reflects the true diffusion ability of water molecules, which decreases with the increase of cell density and the reduction of extracellular space. Secondly, the f value represents the microvascular volume perfusion fraction. Due to the abnormal uneven blood perfusion of neovascularization in malignant tumors, the f value may actually decrease. Also, because of the uneven blood perfusion, there was no significant difference in the D* value in this study.[25–27] Meng et al[28] in the application of amide proton transfer imaging and IVIM sequence to distinguish endometrial polyps from endometrial cancer (EC), research results showed that D and f values in the EC group were significantly lower than those in the endometrial polyps group (D: 0.62 [0.53, 0.76] vs1.45 ± 0.48 [$\times10^{-3}mm^2/s$]; f: 22.18 ± 8.08% vs 30.80 ± 8.92%), which was basically consistent with the results of this study, further verifying the feasibility of non-invasively evaluating benign and malignant nature of tumors using quantitative parameter images of IVIM sequence before surgery.

T2 mapping sequence can reflect relaxation characteristics of water molecules in tissue through T2 value, thereby providing information about the changes in intracellular water content and microstructure.[29] In clinical applications, its value has been verified by many times. For example, Bucher et al[10] in the diagnosis of prostate cancer, T2 mapping can effectively distinguish clinically significant prostate cancer from benign prostate tissue, with an optimal cutoff value of 109.2 ms, providing strong support for precise diagnosis. The results of this study showed that T2 value in the malignant transformation group was significantly lower than that in the benign group, and the difference was statistically significant ($P < .05$). Optimal cutoff value was 119.65 ms, suggesting that T2 value has potential to become a potential biomarker for malignant transformation of EM. This result is consistent with the research conclusion of Li et al.[15] They also observed that in EC, there were significant differences in T2 values among different degrees of malignancy. Changes in T2 values might be related to factors such as tumor cell density and size of extracellular space. When cell proliferation is active and density increases, extracellular space becomes smaller and diffusion of water molecules is restricted, T2 value decreased accordingly.[30] Meanwhile, multivariate logistic regression analysis of this study indicated that T2 value was an independent predictor for evaluating malignant transformation of EM, which further highlighted its important role in predicting early malignant transformation of EM.

Univariate and multivariate logistic regression analyses in this study indicated that D, D* and T2 values were independent predictors for evaluating malignant transformation of EM. It indicates that these MRI parameters can serve as an effective biomarker for monitoring tumor status and can non-invasively provide clinicians with important information regarding risk of malignant transformation of EM. The cutoff values of D, f, and T2 in this study are 1.10×10^{-3} mm^2/s, 37.3%, and 119.65 ms respectively. Values lower than these suggest the possibility of malignant transformation of EM. The combined imaging model constructed with the three parameters is a convenient and objective tool for monitoring the progression of lesions in patients with EM, with good repeatability. It avoids unnecessary surgeries for benign lesions or delayed detection of malignant lesions for patients. In terms of clinical characteristics, laboratory indicator HE4 was the only indicator with statistical difference ($P = .002$). Meanwhile, result of univariate logistic regression analysis (OR = 1.156, $P = .002$) indicated that HE4 was an independent clinical predictor of malignant transformation of EM. This is consistent with the conclusion in the research results of Xu et al[31] that "HE4 is an independent risk factor for diagnosing EAOC." However, this study aimed to construct an imaging parameter model for predicting malignant transformation of EM and did not conduct statistical analysis on clinical-imaging combined indicators.

5. Limitations

The samples of this study were from a single center, and the experimental results were not externally validated through multi-center cases. The next step is to further expand the sample size to verify the corresponding results. Although the diagnostic efficiency of the combined model is relatively high, in practical applications, clinical features and other examination results should be taken into account to improve the accuracy and reliability of diagnosis.

6. Conclusion

IVIM and T2 mapping have significant value in predicting malignant transformation of EM. Their combined model can provide a more comprehensive and accurate risk assessment, offering strong support for the early diagnosis and clinical treatment of patients with malignant transformation of EM.

Author contributions

Conceptualization: Simeng Liu.
Data curation: Simeng Liu, Miao Peng.
Formal analysis: Simeng Liu, Runze Yu.
Funding acquisition: Deli Zhao, Yuhui Deng.
Investigation: Simeng Liu, Cuicui Jin, Shanshan Zhou.
Methodology: Simeng Liu.
Resources: Miao Peng, Runze Yu, Deli Zhao.
Software: Simeng Liu, Cuicui Jin, Shanshan Zhou.
Supervision: Yuhui Deng, Deli Zhao.
Writing – original draft: Simeng Liu.
Writing – review & editing: Yuhui Deng, Deli Zhao.

References

[1] Smolarz B, Szyłło K, Romanowicz H. Endometriosis: epidemiology, classification, pathogenesis, treatment and genetics (review of literature). Int J Mol Sci . 2021;22:10554.
[2] Giannella L, Marconi C, Di Giuseppe J, et al. Malignant transformation of postmenopausal endometriosis: a systematic review of the literature. Cancers (Basel). 2021;13:4026.
[3] Tang L, Bian C. Research progress in endometriosis-associated ovarian cancer. Front Oncol. 2024;14:1381244.
[4] Pejovic T, Thisted S, White M, Nezhat FR. Endometriosis and endometriosis-associated ovarian cancer (EAOC). Adv Exp Med Biol. 2020;1242:73–87.
[5] Wang C, Padgett KR, Su MY, Mellon EA, Maziero D, Chang Z. Multiparametric MRI (mpMRI) for treatment response assessment of radiation therapy. Med Phys. 2022;49:2794–819.
[6] Iima M. Perfusion-driven intravoxel incoherent motion (IVIM) MRI in oncology: applications, challenges, and future trends. Magn Reson Med Sci. 2021;20:125–38.
[7] Cai SQ, Li Y, Li YA, et al. Perfusion-based functional magnetic resonance imaging for differentiating serous borderline ovarian tumors from early serous ovarian cancers in a rat model. Acta Radiol. 2021;62:129–38.
[8] Wang F, Wang Y, Zhou Y, et al. Comparison between types I and II epithelial ovarian cancer using histogram analysis of monoexponential, biexponential, and stretched-exponential diffusion models. J Magn Reson Imaging. 2017;46:1797–809.
[9] Cui YH, Zhu SC, Li HX, et al. Diagnostic value of IVIM for benign and malignant identification of epithelial ovarian tumors and its correlation with Ki67 expression [in chinese]. Chin J Magn Reson Imaging. 2020;11:45–9.
[10] Bucher AM, Egger J, Dietz J, et al. Value of MRI-T2 mapping to differentiate clinically significant prostate cancer. J Imaging Inform Med. 2024;37:3304–15.
[11] Zhu L, Lu W, Wang F, et al. Study of T2 mapping in quantifying and discriminating uterine lesions under different magnetic field strengths: 1.5 T vs. 3.0 T. BMC Med Imaging. 2023;23:1.
[12] Guo JY, Cai YL. Research progress on malignant transformation of ovarian endometriosis. J Southeast Univ (Med Sci Ed). 2024;43:147–51.
[13] Kwon YJ, Shin S, Chun YJ. Biological roles of cytochrome P450 1A1, 1A2, and 1B1 enzymes. Arch Pharm Res. 2021;44:63–83.
[14] Li Y, Zeng X, Lu D, Yin M, Shan M, Gao Y. Erastin induces ferroptosis via ferroportin-mediated iron accumulation in endometriosis. Hum Reprod. 2021;36:951–64.
[15] Li X, Tian S, Ma C, et al. Multimodal MRI for estimating Her-2 gene expression in endometrial cancer. Bioengineering (Basel). 2023;10:1399.
[16] Zheng Z, Zhang S, Zheng C, et al. Qualitative and quantitative features of deep endometriosis in contrast-enhanced ultrasound: an initial experience and literature review. Clin Hemorheol Microcirc. 2023;85:73–82.
[17] Phulia A, Sharma A, Sharma JB, Singh TP, Kumar R. PET/CT imaging in invasive endometriosis: a way to minimize missed diagnosis and reduce invasive interventions. Nucl Med Commun. 2023;44:888–95.
[18] Lashgari M, Yang Z, Bernabeu MO, Li J-R, Frangi AF. SpinDoctor-IVIM: a virtual imaging framework for intravoxel incoherent motion MRI. Med Image Anal. 2025;99:103369.
[19] Zhou M, Chen M, Luo M, Chen M, Huang H. Prognostic factors of rectal cancer based on diffusion-weighted imaging, intravoxel incoherent motion, and diffusion kurtosis imaging. Eur Radiol. 2025;35:979–88.
[20] Tao J, Yin Z, Li X, et al. Correlation between IVIM parameters and microvessel architecture: direct comparison of MRI images and pathological slices in an orthotopic murine model of rhabdomyosarcoma. Eur Radiol. 2023;33:8576–84.
[21] Arian A, Seyed-Kolbadi FZ, Yaghoobpoor S, Ghorani H, Saghazadeh A, Ghadimi DJ. Diagnostic accuracy of intravoxel incoherent motion (IVIM) and dynamic contrast-enhanced (DCE) MRI to differentiate benign from malignant breast lesions: a systematic review and meta-analysis. Eur J Radiol. 2023;167:111051.
[22] Sumi M, Nakamura T. Head and neck tumours: combined MRI assessment based on IVIM and TIC analyses for the differentiation of tumors of different histological types. Eur Radiol. 2014;24:223–31.
[23] Chan SW, Hu WH, Ouyang YC, et al. Quantitative measurement of breast tumors using intravoxel incoherent motion (IVIM) MR images. J Pers Med. 2021;11:656.
[24] Wang Q, Yu G, Qiu J, Lu W. Application of intravoxel incoherent motion in clinical liver imaging: a literature review. J Magn Reson Imaging. 2024;60:417–40.
[25] Luo L, Ye C, Li T, et al. Self-supervised fitting method based on similar neighborhood information of voxels for intravoxel incoherent motion diffusion-weighted MRI. Med Phys. 2025;52:e17825.
[26] Zimmermann J, Reolon B, Michels L, et al. Intravoxel incoherent motion imaging in stroke infarct core and penumbra is related to long-term clinical outcome. Sci Rep. 2024;14:29631.
[27] Rajabi P, Rezakhaniha B, Galougahi MHK, et al. Unveiling the diagnostic potential of diffusion kurtosis imaging and intravoxel incoherent motion for detecting and characterizing prostate cancer: a meta-analysis. Abdom Radiol (NY). 2025;50:319–35.
[28] Meng X, Tian S, Zhang Q, et al. Improved differentiation between stage I-II endometrial carcinoma and endometrial polyp with combination of APTw and IVIM MR imaging. Magn Reson Imaging. 2023;102:43–8.
[29] Hilbert T, Sumpf TJ, Weiland E, et al. Accelerated T2 mapping combining parallel MRI and model-based reconstruction: GRAPPATINI. J Magn Reson Imaging. 2018;48:359–68.
[30] Fujima N, Shimizu Y, Yoneyama M, et al. The utility of diffusion-weighted T2 mapping for the prediction of histological tumor grade in patients with head and neck squamous cell carcinoma. Quant Imaging Med Surg. 2022;12:4024–32.
[31] Xu T, Zhang L, Jiang Y, et al. Clinical characteristics and serum CA19-9 combined with HE4 are valuable in diagnosing endometriosis-associated ovarian cancer. Int J Gynaecol Obstet. 2023;162:472–8.